JOURNAL OF GEOPHYSICAL RESEARCH, VOL. 112, D11111, doi:10.1029/2006JD008093, 2007

A sensitivity study of the coupled simulation of the Northeast Brazil rainfall variability

Vasubandhu Misra[1]

Received 2 October 2006; revised 19 December 2006; accepted 5 March 2007; published 8 June 2007.

[1] Two long-term coupled ocean-land-atmosphere simulations with slightly different parameterization of the diagnostic shallow inversion clouds in the atmospheric general circulation model (AGCM) of the Center for Ocean-Land-Atmosphere Studies (COLA) coupled climate model are compared for their annual cycle and interannual variability of the northeast Brazil (NEB) rainfall variability. It is seen that the solar insolation affected by the changes to the shallow inversion clouds results in large scale changes to the gradients of the SST and the surface pressure. The latter in turn modulates the surface convergence and the associated Atlantic ITCZ precipitation and the NEB annual rainfall variability. In contrast, the differences in the NEB interannual rainfall variability between the two coupled simulations is attributed to their different remote ENSO forcing.

Citation: Misra, V. (2007), A sensitivity study of the coupled simulation of the Northeast Brazil rainfall variability, *J. Geophys. Res.*, *112*, D11111, doi:10.1029/2006JD008093.

1. Introduction

[2] The northeast Brazil (NEB; shown in Figure 1) interannual rainfall variability has received significant attention because of its high predictability [*Misra*, 2006; *Misra and Zhang*, 2006; *Giannini et al.*, 2004, 2001; *Sun et al.*, 2006, 2005; *Folland et al.*, 2001; *Goddard et al.*, 2003]. This arises from the strong forcing on the NEB rainfall variability from the slowly varying SST in the tropical Pacific and the Atlantic Oceans [*Hastenrath and Heller*, 1977; *Moura and Shukla*, 1981; *Nobre and Shukla*, 1996]. Several atmospheric general circulation modeling (AGCM) studies that used observed SST confirmed the observed teleconnections of the NEB rainfall with the eastern equatorial Pacific and the northern tropical Atlantic SST variability [*Misra*, 2004, 2005; *Giannini et al.*, 2001, 2004]. This apparent teleconnection has been exploited with some measured success in providing useful operational seasonal forecasts over the NEB [*Folland et al.*, 2001; *Sun et al.*, 2006].

[3] The annual cycle of precipitation over the NEB is also very robust with a distinct rainy season in February–March–April (February–April) and relatively dry season in August–September–October (August–October; *Misra* [2006]; *Kayano and Andreoli* [2006]). This robust annual cycle of the NEB rainfall is largely dictated by the annual meridional march of the precipitation associated with the Atlantic intertropical convergence zone (ITCZ) across the equator [*Nobre and Shukla*, 1996]. The meridional migration of the Atlantic ITCZ precipitation across the equator is governed by several factors including the annual cycle of the solar insolation, the coastal geometry, the meridional gradient of SST, the magnitude of in situ SST, and surface convergence [*Biasutti et al.*, 2005, 2004, 2003; *Li and Philander*, 1997; *Philander et al.*, 1996].

[4] In the novel experiments of *Li and Philander* [1997] it was shown that the changes in the surface winds (especially in its north-south component) induced by the seasonal change of the land surface temperatures in west Africa modulate a strong seasonal cycle of SST in the eastern Atlantic Ocean. While in the western Atlantic Ocean the coupled ocean-atmosphere interactions seemed to play a dominant role in the annual cycle of SST. Furthermore, *Philander et al.* [1996] indicated that the asymmetry of tropical Atlantic SST about the equator was primarily a result of the bulge of the African continent to the north of the Gulf of Guinea while the stratus clouds played a secondary role of amplifying this asymmetry further.

[5] The objective of this study is to understand the role of the shallow inversion clouds (SIC; also commonly referred as marine boundary layer or stratus clouds) on the robust annual cycle and interannual variability feature of the NEB precipitation. This is achieved by analyzing two multidecadal simulations of the Center for Ocean-Land-Atmosphere Studies (COLA) coupled climate model which differ from each other in its parameterization of the SIC in its atmospheric general circulation model (AGCM) component. In effect, the differences in these coupled simulations will reveal the influence of the SIC found mainly in the subtropical regions of the open oceans.

[6] As we progress in adopting a fully coupled dynamical model for operational forecasting [*Saha et al.*, 2006], well-observed teleconnection patterns serve as invaluable measures for validating the variability in such coupled modeling systems. *Misra and Zhang* [2006] showed that in the National Centers for Environmental Prediction (NCEP) climate

[1]Center for Ocean-Land-Atmosphere Studies Institute of Global Environment and Society, Inc., Calverton, Maryland, USA

0148-0227/07/2006JD008093$09.00

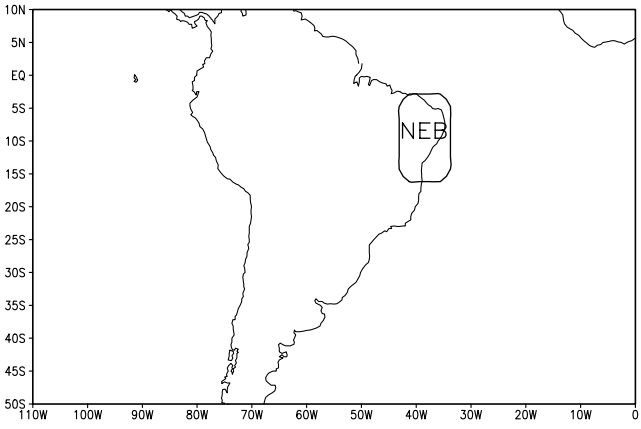

Figure 1. The outline of northeast Brazil (NEB).

forecast system (a fully coupled ocean-land-atmosphere model) the seasonal prediction skill of the NEB rainy season (Feb–Apr) even at zero lead time is poor compared to some of the earlier modeling studies that used observed SST. This deterioration of the skill in the NCEP climate forecast system was attributed to an erroneous El Niño Southern Oscillation (ENSO) forcing over the tropical Atlantic Ocean. As a result the meridional gradient of the tropical Atlantic SST anomalies, a critical forcing parameter of the NEB rainfall variability was found to be erroneous in the NCEP climate forecast system. Therefore in the context of the NCEP climate forecast system and other such coupled systems it is important to understand the sensitivity of such teleconnections to model parameters. This study is motivated in isolating one such model parameter (parameterization of the SIC) that seems to play a significant role in determining the teleconnection of the NEB rainfall variability in the Center for Ocean-Land-Atmosphere Studies (COLA) coupled climate model.

[7] Fundamentally, the NEB rainfall variability is strongly dictated by the variability in the marine Atlantic intertropical convergence zone (ITCZ; *Nobre and Shukla* [1996]; *Giannini et al.* [2004]). Typically, it is seen that in warm (cold) ENSO events with concomittant warm (cold) SST anomalies over the northern tropical Atlantic Ocean [*Enfield and Mayer*, 1997], the ITCZ is stronger (weaker) over the northern tropical Atlantic Ocean thereby decreasing (increasing) the February–March–April (February–April; rainy) seasonal mean rainfall over the NEB [*Moura and Shukla*, 1981; *Hastenrath and Heller*, 1977]. There is however, growing evidence to indicate that this teleconnection does not always hold true [*Kayano and Andreoli*, 2006; *Giannini et al.*, 2004; *Misra*, 2005]. It is seen that when the tropical Atlantic SST anomalies (especially north of the equator) develop contrary to the external forcing of ENSO, predictability of the NEB is reduced [*Giannini et al.*, 2004; *Misra*, 2005]. Such intrinsic SST anomalies over the tropical Atlantic are generated from the local coupled ocean-atmosphere mode, and are comparable to the external forcing of ENSO [*Chang et al.*, 2003]. In this study, however, we will limit ourselves in understanding how the SIC influences the ENSO teleconnection with the NEB rainfall variability.

[8] In the following section the COLA coupled model is briefly discussed followed by a brief description of the conducted experiments. Results are presented in section 4 followed by a discussion and concluding remarks in section 5.

2. Model Description

[9] The recently developed COLA coupled climate model [*Misra et al.*, 2006] is used in this study. The AGCM is used at a spectral resolution of T62 (≈200 km grid resolution) with 28 sigma ($=\frac{p}{p_s}$) levels. A brief outline of the AGCM is provided in Table 1. The readers are referred to the work of *Misra et al.* [2006] for a detailed description of the AGCM. This AGCM is coupled to the modular ocean model version 3.0 (MOM3; *Pacanowski and Griffies* [1998]). MOM3 has a uniform zonal resolution of 1.5° while the meridional resolution is 0.5° between 10°S and 10°N gradually increasing to 1.5° at 30°N and 30°S and fixed at 1.5° in the extratropics.

3. Design of Experiments

[10] Two separate coupled simulations are conducted over a 70-year period, each with slightly different parameterization of the SIC. Fundamentally, the parameterization of the SIC follows from *Kiehl et al.* [1998]. The fraction of the SIC (C_{inv}) is determined from:

$$C_{\text{inv}} = -6.67\left[\left(\frac{\partial\theta}{\partial p}\right) - \left[\frac{\partial\theta}{\partial p}\right)_{\text{c}}\right] \times \text{RHf} \tag{1}$$

where, $\left(-\frac{\partial\theta}{\partial p}\right)_c$ is the critical lapse rate that must be exceeded for SIC to be diagnosed (in our case it is 4×10^{-2} deg/Pa). RHf is a function of the relative humidity given by:

$$0.0 \text{ if } \text{RH} < 0.6$$

$$1.0 - \tfrac{(0.8-\text{RH})}{0.2} \text{ if } 0.6 \leq \text{RH} \leq 0.8$$

$$1.0 \text{ if } 0.8 < \text{RH}$$

[11] In addition, the SIC scheme is not invoked at a grid point if convection is active at the same given time step. The generated SIC are then used to diagnose the total cloud fraction using maximum overlap between clouds. Generally, this algorithm produces SIC in 900–700 hPa layer in the vertical over the open oceans of the tropics. In the control (CONTROL) coupled simulation of this study the fraction of SIC diagnosed from the above methodology are smoothed using a three-point filter ($C^{\text{f}}_{\text{inv}}$):

$$C^{\text{f}}_{\text{inv}} = \left[0.25C^{i+1}_{\text{inv}} + 0.5C^{i}_{\text{inv}} + 0.25C^{i-1}_{\text{inv}}\right] \tag{2}$$

where i refers to any given grid point in the longitudinal direction of the AGCM. The filter is used in the CONTROL to reduce the spectral effects on low level clouds (especially SIC) generated by the spectral effects in the prognostic fields of the AGCM. The smoothing was done only in the

Table 1. The Outline of the COLA AGCM Used in This Study

Process	V3.2
Advection	Dynamical core [*Kiehl et al.*, 1998]; dependent variables are spectrally treated except for moisture which is advected by semi-Lagrangian scheme
Deep Convection	Relaxed Arakawa Schubert scheme [*Bacmeister et al.*, 2000]
Longwave Radiation	*Collins et al.* [2002]
Boundary Layer	Nonlocal [*Hong and Pan*, 1996]
Land Surface Process	*Xue et al.* [1991, 1996]; *Dirmeyer and Zeng* [1999]
Shallow Convection	*Tiedtke* [1984]
Shortwave Radiation	*Briegleb* [1992]
Diagnostic Cloud Fraction and Optical Properties	*Kiehl et al.* [1998]

longitudinal direction because of practical constraints in coding filters that involved smoothing across latitudes. The COLA AGCMV3.2 (similar to other AGCMs) is coded to run in distributed memory systems using message passing interface (MPI) programs that slices the global array of discrete grid points along longitudes and depth before it is sent out to different processors for computing grid point physics. Therefore computations across latitudes in the physics of the AGCM is cumbersome and rather impractical. Furthermore, we found that by filtering only in the longitudinal direction, the apparent noise observed especially in the downwelling shortwave flux is considerably reduced compared to EXPT, in which no filter was applied to the SIC.

[12] In EXPT the absence of any smoothing to SIC produces spatially incoherent SIC. As a consequence the downwelling shortwave flux is reduced in the open oceans considerably in the CONTROL compared to EXPT. However, at the margins of the SIC especially along the coast the smoothing leads to optically thin clouds and thereby increasing the downwelling shortwave flux relative to EXPT. This is illustrated in Figure 2 which shows the climatological downwelling shortwave flux for February–April and August-October seasons from the CONTROL and its corresponding difference from EXPT simulations.

[13] It should be noted that the spectral effects on clouds are more apparent in the current version of the COLA AGCM than in the earlier versions of the COLA AGCM [*Schneider*, 2002] primarily because the fourth order horizontal diffusion coefficient has been reduced from 2.5×10^{16} m^4 s^{-1} to 1.0×10^{14} m^4 s^{-1}, a change of two orders of magnitude. Furthermore, the orography was changed to that in NCEP reanalysis model [*Kalnay et al.*, 1996] which has sharper gradients than that used in the earlier version of the COLA AGCM [*Fennessy et al.*, 1994]. The new diffusion coefficient represents the least that the model can handle without becoming numerically unstable when integrated for long periods.

[14] Each of the coupled experiments signify a plausible distribution of the SIC that could arise as a result of:

[15] 1. The choice of orography (smoothed or enhanced) in the AGCM or

[16] 2. The choice of the horizontal diffusion coefficient if such explicit control of the horizontal diffusion is possible.

[17] 3. The choice of the dynamical core when some schemes are implicitly more diffusive than others.

[18] 4. The choice of the horizontal and vertical resolution of the AGCM that can highlight the spectral effect as a result of the "on-off" switches in the parameterization scheme.

[19] The ocean model was integrated from the initial state of rest with initial conditions of temperature and salinity of *Levitus* [1982], and forced with climatological wind stress derived from the special sensor microwave imager (SSMI) for a period of 100 years. Thereafter, each of the coupled simulations was integrated for a period of 70 years. The results in this study are analyzed from the last 45 years of the integration discarding, the first 25 years as a spin-up period of the coupled model.

4. Results

[20] The results from the coupled model simulations are compared with the extended reconstructed SST version2 (ERSST2; *Smith and Reynolds* [2003]), NCEP-NCAR reanalysis [*Kalnay et al.*, 1996] made available at T62 spectral truncation grid for surface variables and at 2.5° grid resolution for atmospheric variables, and precipitation from the Climate Prediction Center Merged Analysis Precipitation (CMAP; *Xie and Arkin* [1996]) at 2.5° lat/long grid resolution. It should be noted that the period 1955–2000 for ERSST2 and NCEP-NCAR reanalysis are used for verification of the 45 years of coupled model integration. For CMAP, 27 years of observational coverage from 1979–2005 is used to verify the coupled simulations. However, we have used the overlapping periods only when CMAP and ERSST2 are used together for creating observed teleconnection patterns. In the following subsections we will highlight the differences between the simulations in the context of the annual cycle of the NEB rainfall variability followed by results on interannual variability.

4.1. Annual Cycle

4.1.1. The Annual Cycle of Precipitation Over the Northeast Brazil

[21] In Figure 3 the annual cycle of precipitation over the NEB is shown from CMAP (OBS), CONTROL, and EXPT. The annual cycle of observed precipitation over the NEB is robust with a distinct maximum in February-April season and a minimum in August-October season. The CONTROL and EXPT are able to reasonably simulate this annual cycle. However, a wet (dry) bias is observed in the CONTROL (EXPT) in the wet season of February–April. Similarly dry bias exists in the dry August–October season in both the coupled simulations. It should be noted that the domain of the NEB shown in Figure 1 extends into northern and southern Nordeste which exhibit slightly different annual cycle [*Nobre and Shukla*, 1996]. This subtlety is not resolved at the coarse spatial resolution of the AGCM and the observations (CMAP and NCEP reanalysis) used in this

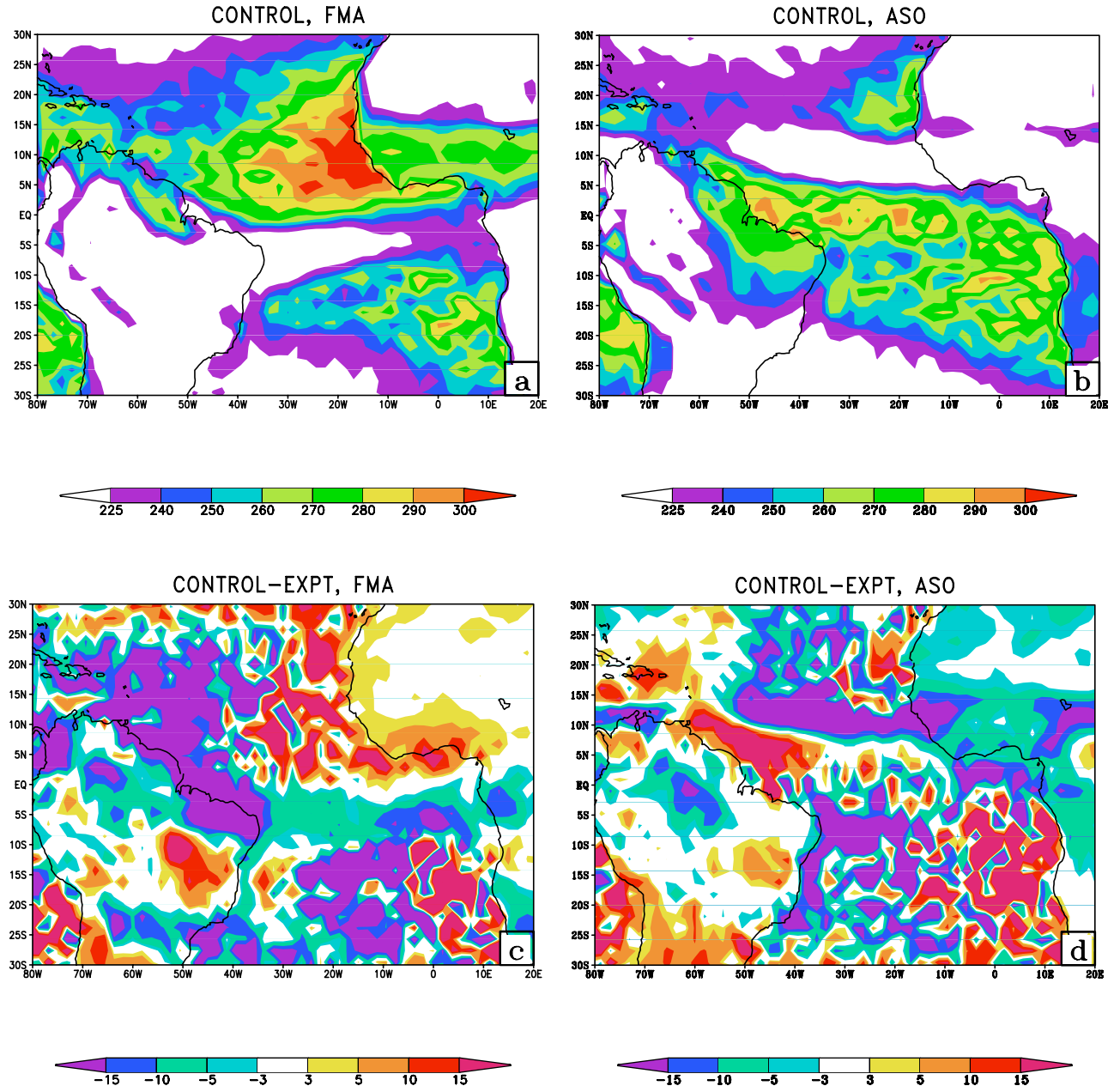

Figure 2. Climatological FMA and ASO seasonal mean downwelling shortwave flux at surface from (a, b) CONTROL and their corresponding difference with (c, d) EXPT. The units are in Wm^{-2}.

study. Furthermore, choosing a smaller domain than indicated in Figure 1 will grossly undersample the model features in the domain relative to its horizontal resolution.

4.1.2. The Annual Cycle of Precipitation in the Tropical Atlantic Ocean

[22] As mentioned earlier, the annual cycle of precipitation over the NEB is intricately related to the seasonal migration of the marine Atlantic ITCZ. In Figures 4a and 4b the zonally averaged (between 45°W and 10°E) precipitation is shown from observations (OBS; CMAP) and the CONTROL simulation respectively. The observed seasonal meridional migration of the ITCZ from the southern tropical Atlantic latitudes in the NEB wet season to the northern tropical latitudes in the NEB dry season is reasonably well simulated in the CONTROL. In addition, the location of the maximum precipitation (albeit stronger than observations) centered around 10°N in the August–October season is also a highlight of the CONTROL simulation. However, the common problem of most AGCMs and coupled models of having erroneously strong convection south of the equator [*Biasutti et al.*, 2006] is also seen in the CONTROL simulation. As observed in other models the CONTROL extends the Atlantic ITCZ too far to the south relative to the observations especially in the Boreal spring season of March–April–May. In Figure 4c the difference of the CONTROL simulation from the corresponding precipitation of EXPT is shown. The changes to the SIC in the CONTROL simulation has reduced the precipitation significantly to the south of the equator relative to the EXPT (Figure 4c). Likewise, in Figure 4c the CONTROL simulation has

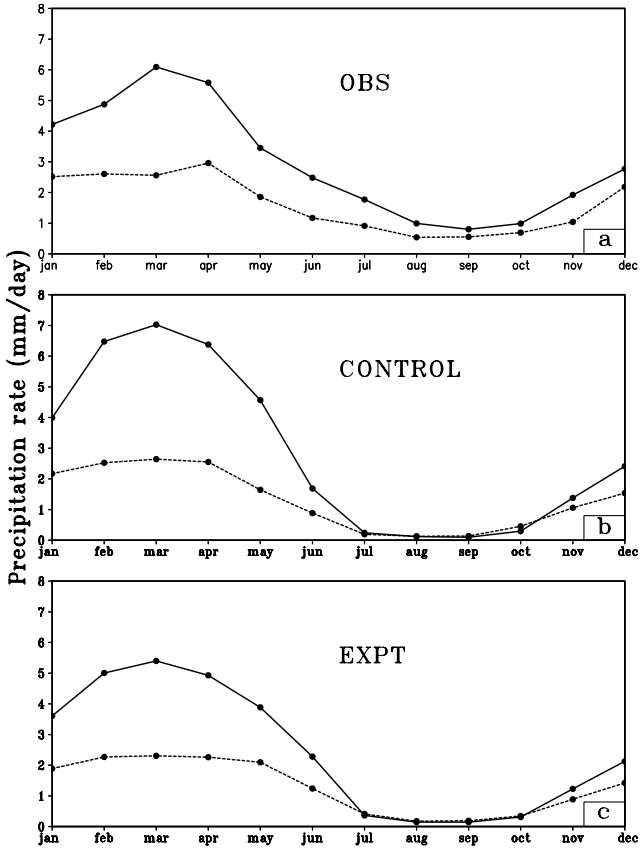

Figure 3. The annual cycle of precipitation (solid line; units are in mm day^{-1}) and interannual standard deviation (dotted line) over northeast Brazil from (a) OBS (CMAP), (b) CONTROL, and (c) EXPT simulations.

increased the precipitation north of the equator relative to the EXPT. Furthermore, there is an asymmetry in the response in that the differences between the CONTROL and the EXPT precipitation are relatively much larger in the NEB dry season of August–October.

4.1.3. Thermodynamic Control Versus Dynamic Control

[23] *Biasutti et al.* [2006] made the distinction of the AGCMs that exhibited the primary mechanism of precipitation over the tropical Atlantic Ocean between that from thermodynamic control (wherein the precipitation is determined locally by SST; *Raymond et al.* [2003]; *Neelin and Su* [2005]) and that from dynamic control (wherein the surface convergence is the determining factor of precipitation; *Lindzen and Nigam* [1987]; *Tomas et al.* [1999]). It is to be recognized however that precipitation in either of these class of models do not exclusively occur because of one of the controls but the classification is based on the preponderance of one of the controls. *Biasutti et al.* [2006] showed that many of the AGCMs exhibited erroneously a strong thermodynamic control of precipitation as determined from the colocation of maximum precipitation with maximum SST over the tropical Atlantic Ocean. This feature is examined in the OBS, NCEP reanalysis, CONTROL, and EXPT for the two contrasting seasons of the NEB annual cycle of rainfall namely, February–April and August–October. In Figures 5a and 5b the observations show the maximum precipitation in the February–April (August–October) season over the western (eastern) Atlantic in eastern Brazil (Sahel and Gulf of Guinea) while the maximum SST is in the eastern (western) Atlantic Ocean over the Gulf of Guinea (Carribbean Sea). The corresponding NCEP reanalysis in Figures 5c and 5d show qualitatively a similar feature. However, in August–October season the NCEP reanalysis produces copious amount of precipitation over tropical South America that is unsupported from observations. The CONTROL simulation in Figures 5e and 5f also does not colocate the maximum precipitation with the maximum SST. However, the southward extension of a strong ITCZ (south of 10°S) and the appearance of very warm SST in the Gulf of Guinea in Figure 5e, and the presence of the cold equatorial tongue in Figure 5f are some of the apparent biases of the CONTROL simulation. However, the EXPT (Figures 5g and 5h) unlike the CONTROL, colocates maximum precipitation with maximum SST in both the February–April and the August–October seasons. It is also apparent from the figure that the warm bias in the February–April season over the tropical Atlantic Ocean is relatively much larger in the EXPT than in the CONTROL simulation. In comparing Figures 2 and 5 it can be seen that warmer (colder) SSTs in the EXPT is a direct result of the increase (decrease) in the downwelling shortwave flux at the surface relative to the CONTROL. For the same reason, in the August–October season the bias of the equatorial cold tongue is larger in the CONTROL than in the EXPT.

[24] Similar to Figure 5 the surface wind (1000 hPa) wind divergence is displayed with corresponding precipitation from the NCEP reanalysis, CONTROL, and the EXPT simulation for both the February–April and the August–October seasons in Figure 6. It is apparent from the figure that maximum precipitation in the NCEP reanalysis, the CONTROL, and the EXPT is colocated with the maximum surface convergence. However, there is a reduction in magnitude of the surface convergence in EXPT compared to the CONTROL simulation. This may intuitively explain the decrease in the intensity of the precipitation over the Atlantic ITCZ in the EXPT relative to the CONTROL simulation. It should be noted that the column integrated moisture flux convergence is also colocated with surface convergence and precipitation in the coupled simulations and in the NCEP reanalysis over the Atlantic ITCZ (not shown).

[25] The larger precipitation difference over the Atlantic ITCZ between the CONTROL and the EXPT in the August–October season (see Figure 4) relative to the February–April season is because the latitude of maximum surface convergence shifts from 10°N in the CONTROL to 7°N in the EXPT in the August–October season causing a much larger change in the surface convergence. In contrast, in the February–April season the latitude shift is not apparent and the ITCZ remains at around 6°S in the two simulations (CONTROL and EXPT), while the magnitude of the surface convergence changes between the two simulation over the western Atlantic Ocean as a result of the changes in the wind speed.

4.1.4. Modulation of Surface Pressure Gradient

[26] It is apparent that maximum precipitation over the Atlantic ITCZ tends to colocate with maximum surface

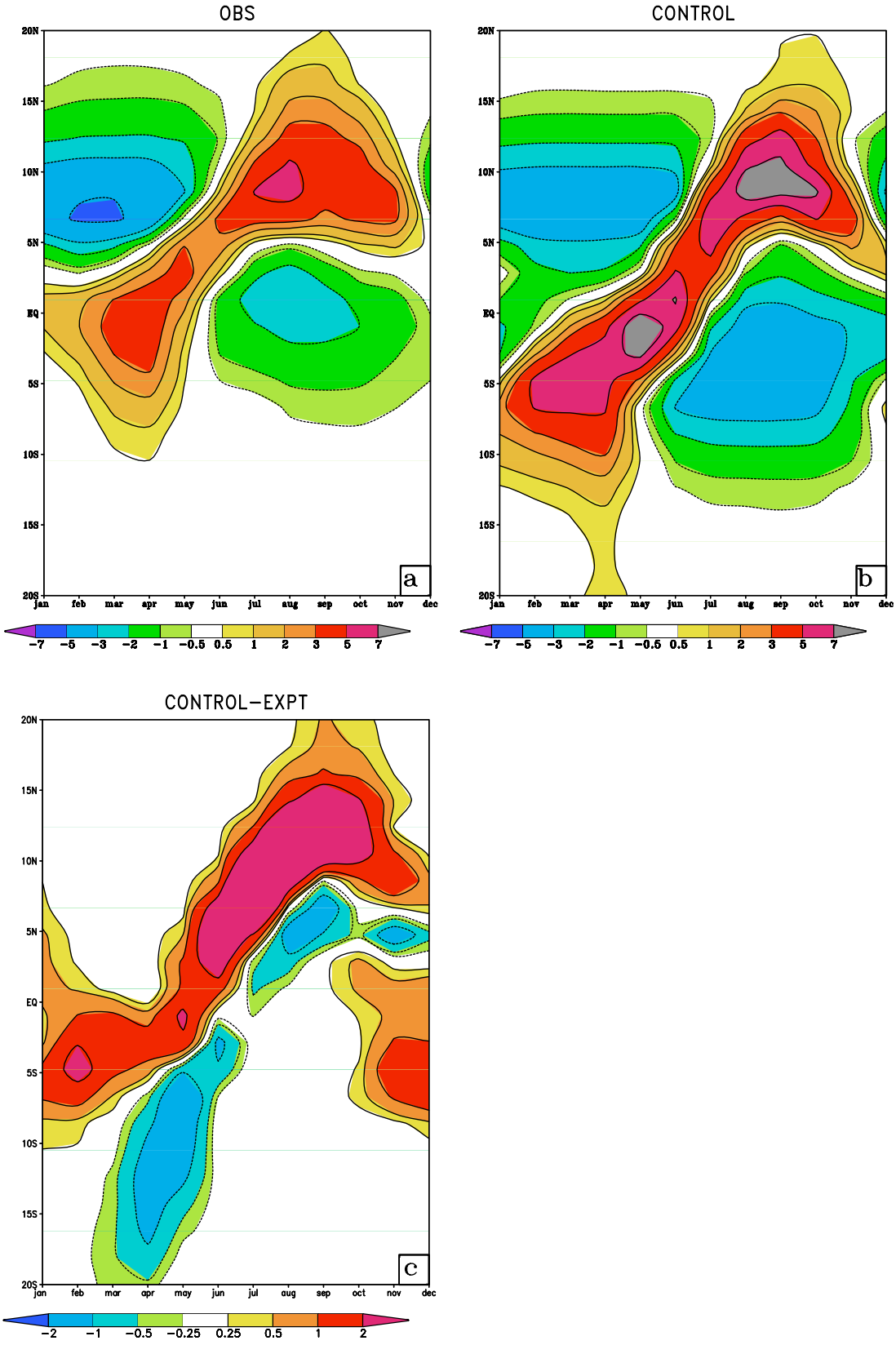

Figure 4. The climatological annual cycle of zonally averaged (between 45±W and 10±E) precipitation (in mm day^{-1}) after removing the annual mean from the (a) observations (CMAP), (b) CONTROL, and (c) difference between CONTROL and EXPT.

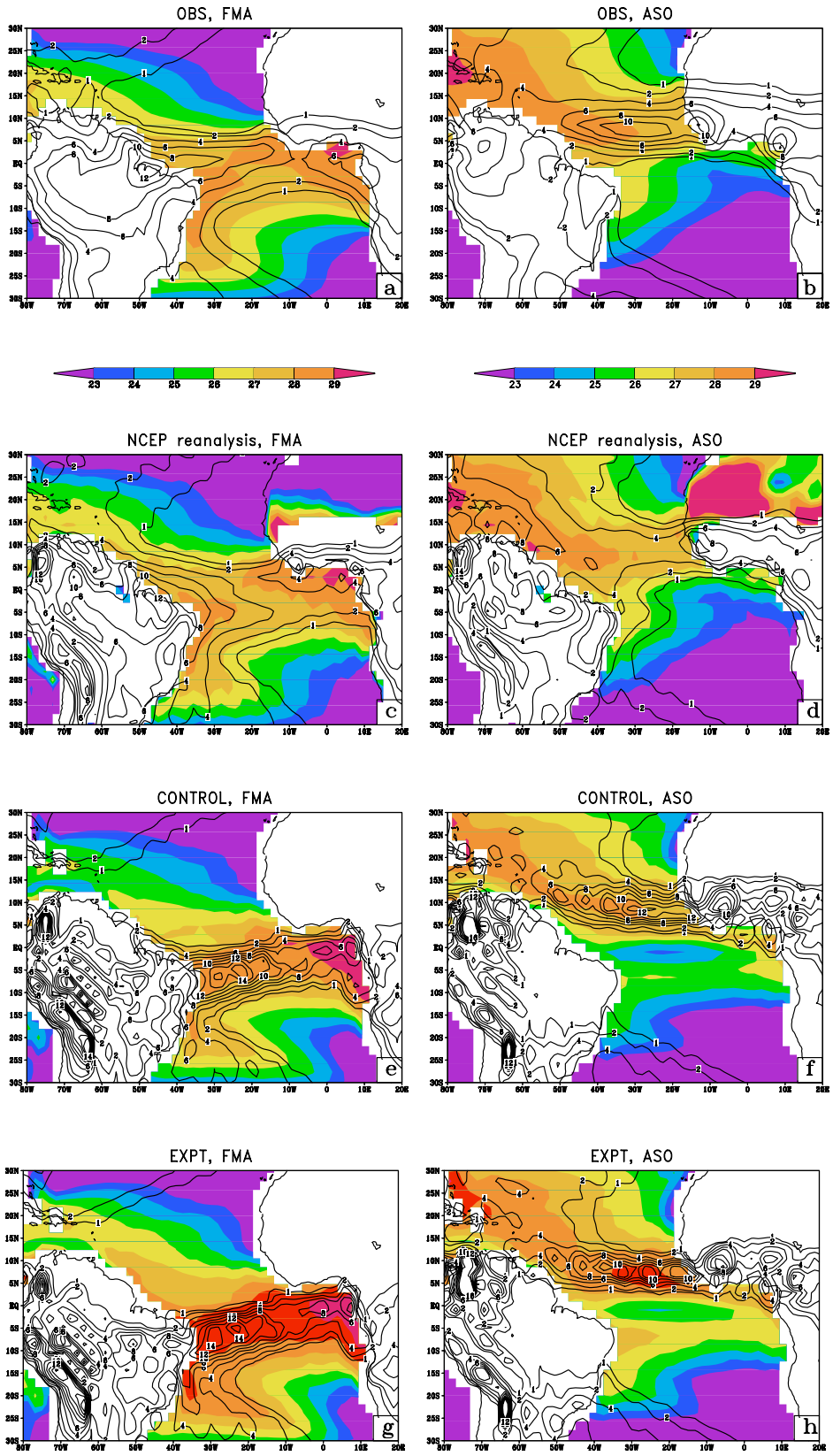

Figure 5. Climatological FMA and ASO seasonal mean SST(shaded) and precipitation (contoured) from (a, b) OBS (ERSSTV2 and CMAP) (c, d) NCEP reanalysis, (e, f) CONTROL, and (g, h) EXPT. The units of SST and precipitation are in °C and mm day^{-1}, respectively. The SST in Figures 5c and 5d are from ERSSTV1.1.

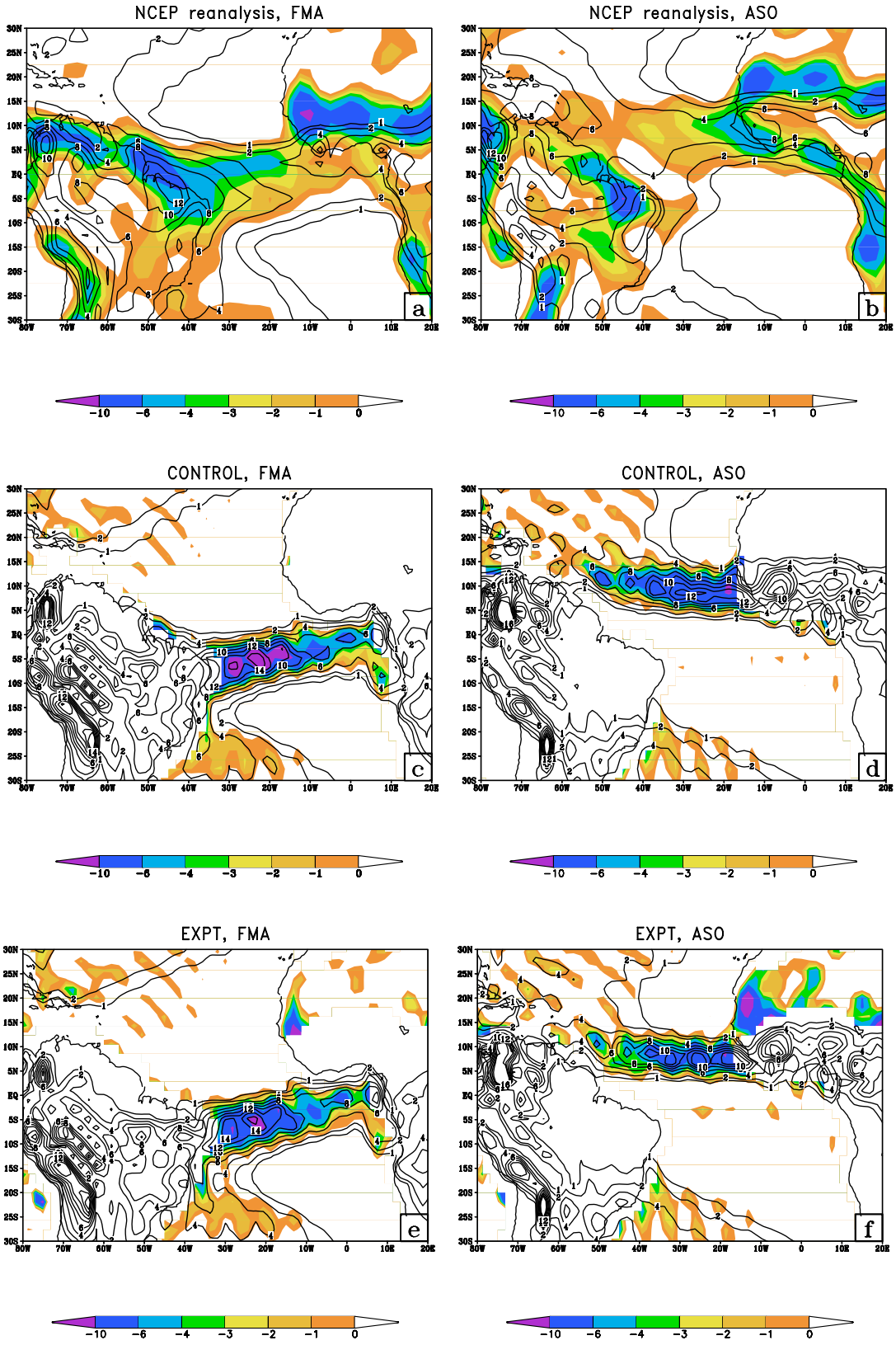

Figure 6. Climatological FMA and ASO seasonal surface convergence (only negative values are shaded) at 1000 hPa overlaid with corresponding precipitation (contoured) from (a, b) NCEP reanalysis, (c, d) CONTROL, and (e, f) EXPT simulations. The units of convergence and precipitation are 1×10^{-6} s^{-1} and mm day^{-1}, respectively. The 1000-hPa convergence over land is undefined for the CONTROL and EXPT simulations as it lies below the model orography. Corresponding NCEP reanalysis values over most land regions may be ignored for the same reason.

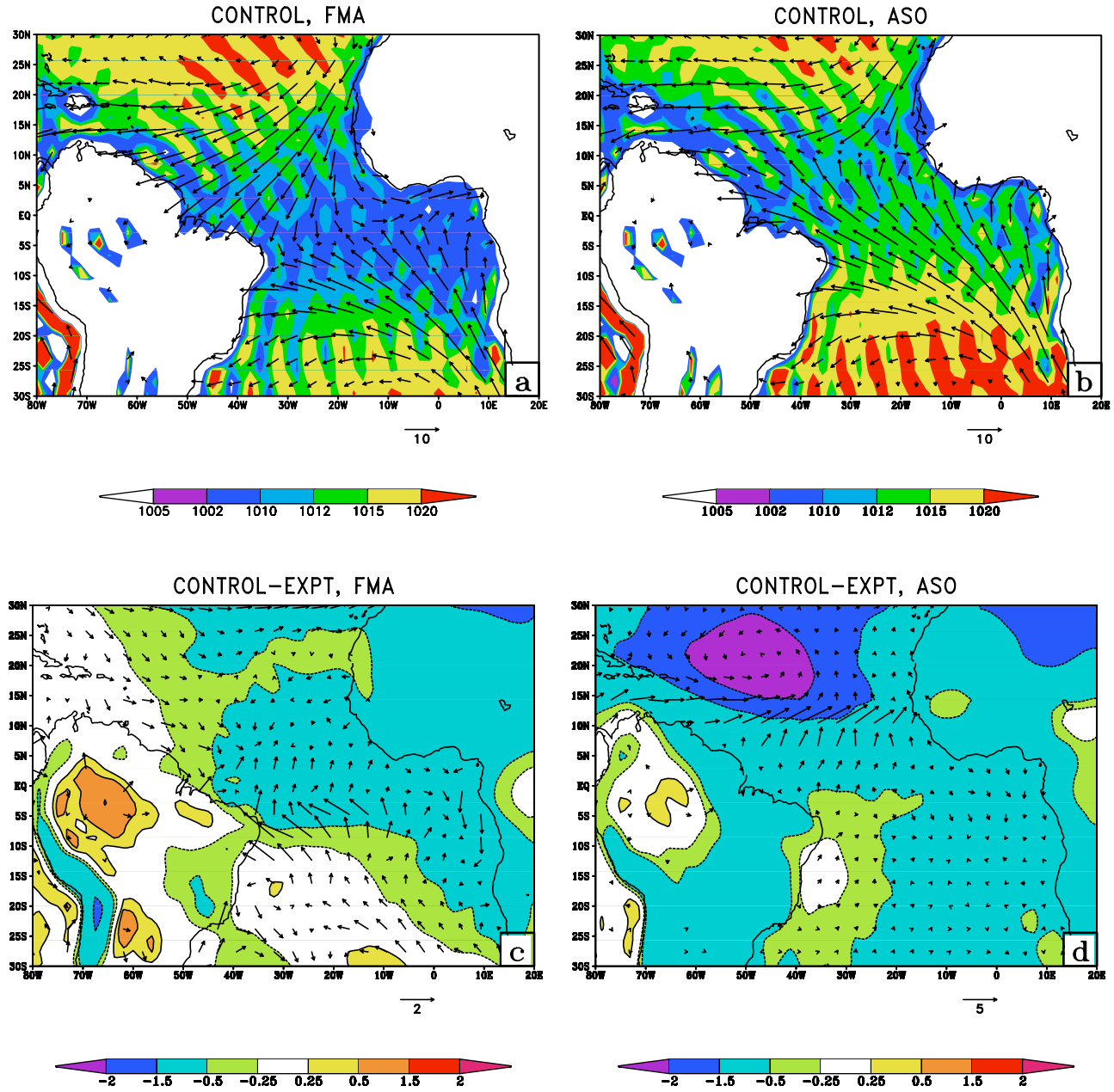

Figure 7. FMA and ASO seasonal mean surface pressure (shaded) and 1000 hPa winds from (a, b) CONTROL and (c, d) its corresponding difference from EXPT. The units of surface pressure and winds are in hPa and ms^{-1}, respectively.

convergence rather than over maximum SST both in the NCEP reanalysis and in the coupled simulations. Furthermore, the the CONTROL simulation showed more precipitation over the tropical Atlantic as a result of the increase in surface convergence relative to the EXPT which had higher in situ SST.

[27] The differences in the surface convergence between the two coupled simulations of this study occur primarily as a result of the changes to the surface pressure gradient which is a consequence of its synergistic relationship with deep convection. It is important to understand that there is a positive feedback mechanism in play with deep convection heating the atmosphere, lowering the surface pressure, and enhancing the surface convergence which is ultimately compensated by the annual march of the solar insolation. This modulation of the surface pressure gradient is illustrated in Figures 7a and 7b which shows the surface pressure and 1000 hPa winds from the CONTROL simulation for February–April and August–October seasons, respectively. Their corresponding differences from EXPT are shown in Figures 7c and 7d. In February–April the surface convergence is stronger in the CONTROL over the western Atlantic Ocean just offshore of the NEB. This is primarily facilitated by the meridional component of the surface wind that responds to the stronger meridional surface pressure gradient in the CONTROL simulation

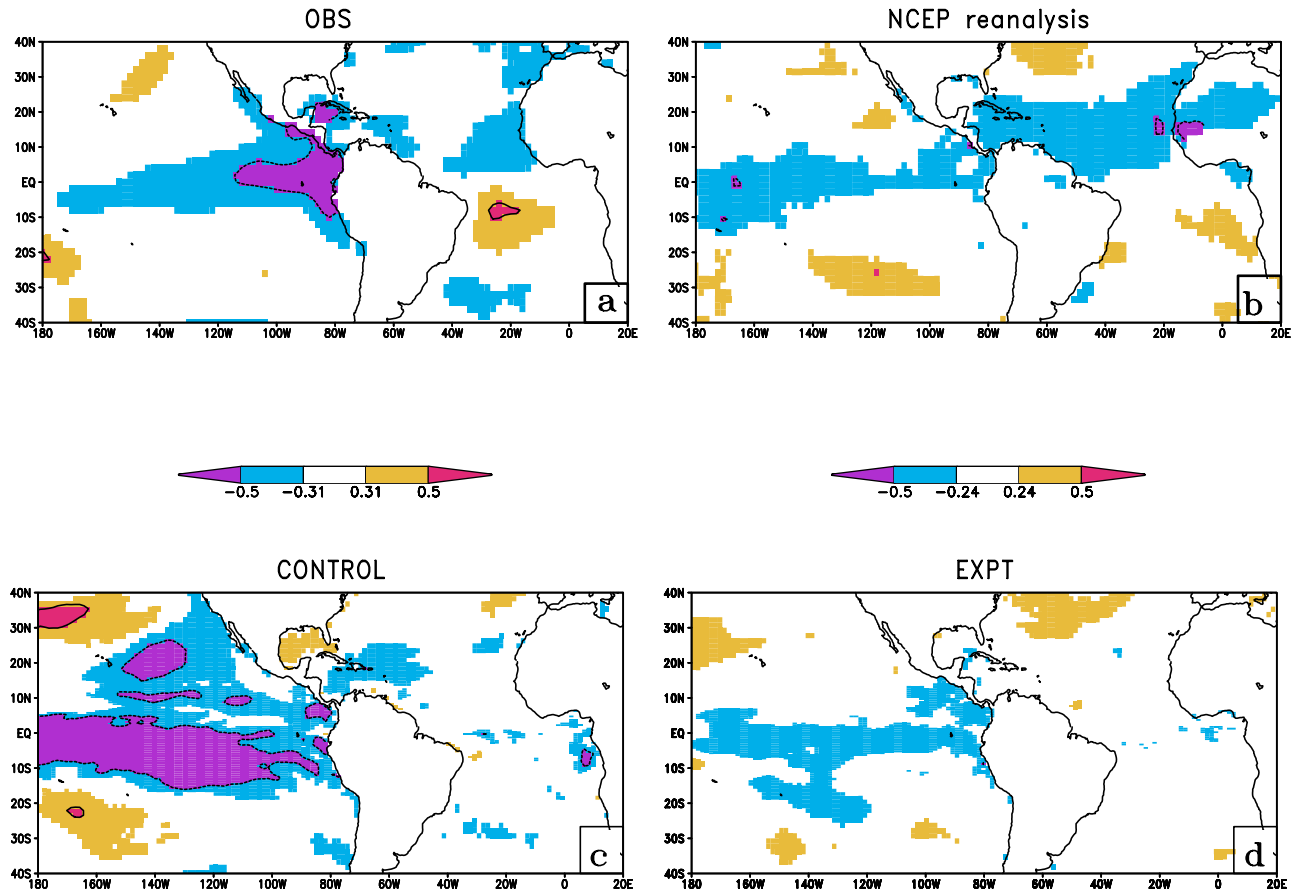

Figure 8. The correlation of FMA seasonal precipitation anomaly over the NEB with contemporaneous SST from (a) OBS, (b) NCEP reanalysis, (c) CONTROL, and (d) EXPT simulations. Values that exceed 90% confidence interval according to *t* test are shown. Since the period used in OBS is 27 years (1979–2005) while for the rest it is 45 years the confidence intervals are slightly different in Figure 3a. Precipitation anomaly over the NEB with contemporaneous SST from (a) OBS, (b) NCEP reanalysis, (c) CONTROL, and (d) EXPT simulations. Values that exceed 90% confidence interval according to *t* test are shown.

relative to EXPT. In Figure 7c, the CONTROL has lower (higher) pressure in the equatorial (subtropical south) Atlantic Ocean thereby increasing the meridional surface pressure gradient relative to the EXPT in the February–April season. In the August–October season, however, there is a latitudinal shift of the convergence zone (with the ITCZ moving further northward in the CONTROL relative to the EXPT) with associated changes in the surface pressure gradient between the CONTROL and the EXPT. This results in much larger change in precipitation over the ITCZ in August–October compared to February–April between the two coupled simulations.

[28] It becomes obvious now that despite the increase in SST over the tropical Atlantic Ocean in the EXPT compared to the CONTROL simulation, the rainy season over the NEB is climatologically less intense as a result of the reduced surface convergence. Furthermore, the dry bias in August–October over the NEB is similar in the EXPT and in the CONTROL even though the Atlantic ITCZ exhibits large differences between the coupled simulations. This is because the ITCZ in the August–October season is at its northern most position of its annual cycle, remote from NEB.

4.2. Interannual Variability

4.2.1. The Phase Locking of Interannual Variability to Annual Cycle

[29] In Figures 3a–3c the annual cycle of the monthly mean precipitation over the NEB along with its standard deviation is shown from CMAP (OBS), CONTROL, and EXPT, respectively. It is evident from Figure 3 that the interannual variability of the rainfall peaks in the February–April season and reaches a nadir in the August–September–October (August–October) season, in phase with the annual cycle. This annual cycle of the interannual variability of precipitation over the NEB is rather well maintained in both the CONTROL and the EXPT coupled simulations. However, in the EXPT it has an erroneous feature of showing higher variability in May compared to the OBS and the CONTROL. Moreover, both simulations display weaker variability in Boreal fall season of August–October compared to the observations.

4.2.2. Teleconnection Associated With the NEB Rainfall Variability

[30] The well established negative correlation of the February–April seasonal NEB precipitation anomalies with

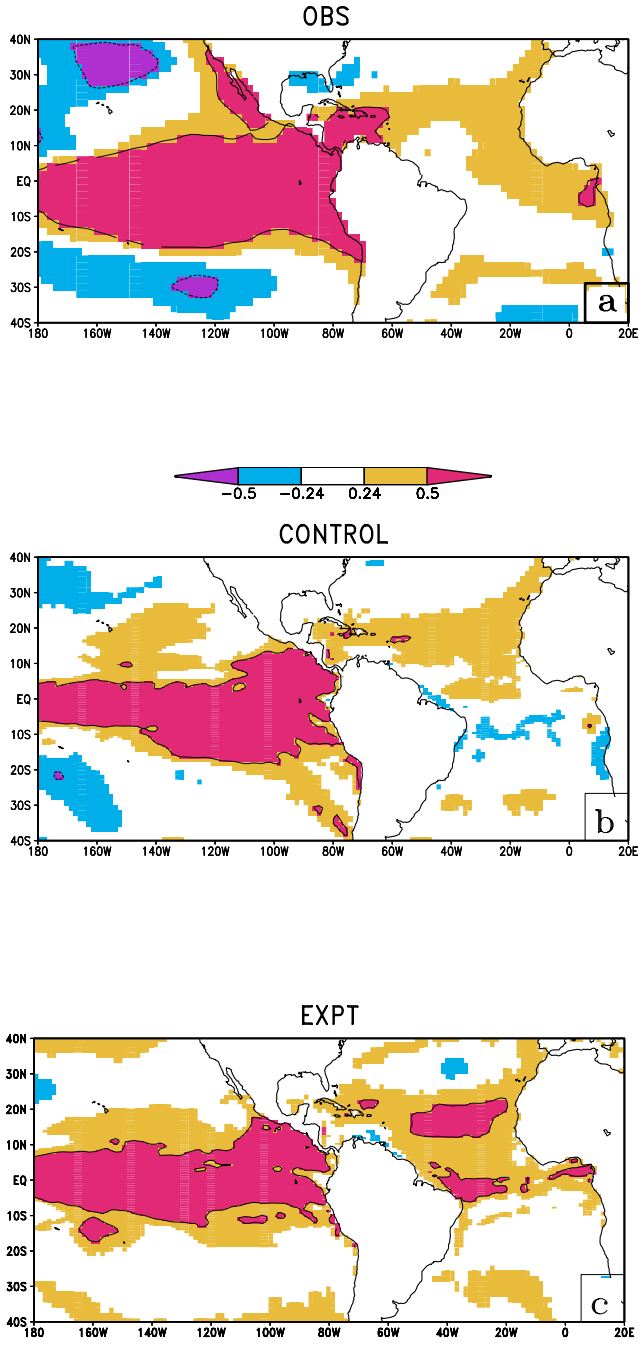

Figure 9. The contemporaneous correlation of the Niño3 SST index averaged over the FMA season with the corresponding global SST from (a) OBS, (b) CONTROL, and (c) EXPT coupled simulations. Values that exceed 90% confidence interval according to *t* test are shown.

the corresponding SST anomalies in the eastern equatorial Pacific and northern tropical Atlantic Oceans is clearly seen from the OBS in Figure 8a and further corroborated in the NCEP reanalysis in Figure 8b. It should be noted that the significant positive correlations that appear in the south tropical Atlantic Ocean in Figure 8a have also been observed in other studies [*Misra*, 2005; *Kayano and Andreoli*, 2006]. This feature is not captured in either of the coupled simulations. *Kayano and Andreoli* [2006] identify these SST anomalies to intrinsic modes of the south tropical Atlantic that exert their influence on the NEB rainfall in February–April season independent of the variability from the tropical Pacific Ocean. The cause for the appearance of these SST anomalies over the subtropical South Atlantic region is still in debate: it is either related to ENSO via a Pacific-South American teleconnection pattern [*Mo and Higgins*, 1998; *Cazes-Boezio et al.*, 2003] or a result of intrinsic variability [*Huang et al.*, 2005]. The CONTROL simulation (Figure 8c) exhibits this teleconnection with significant correlations appearing in the eastern equatorial Pacific and the northern tropical Atlantic regions. On the other hand, the NEB seasonal February–April precipitation anomalies in the EXPT simulation displays teleconnection only over the eastern equatorial Pacific region. Consequently the correlations of the February–April seasonal rainfall over the NEB between the CONTROL and EXPT is very small (0.08).

4.2.3. Covariability of Niño3 SST Index With the Tropical Atlantic

[31] In Figures 9a and 9b the contemporaneous correlation of the Niño3 SST index with the tropical Pacific and Atlantic SST anomalies is shown. The positive correlations over the northern tropical Atlantic region are evident in the OBS and in the CONTROL simulation. However, in the EXPT contrary to the OBS and the CONTROL, the positive correlations extend into both hemispheres in the tropical Atlantic Ocean. This erroneous feature was also observed in the NCEP climate forecast system [*Misra and Zhang*, 2006]. This form of external forcing in the tropical Atlantic region from the eastern equatorial Pacific in the EXPT leads to a modulation of the gradient of the SST anomalies, which manifests itself in the absence of any significant correlation of the NEB rainfall variability with the SST anomalies in the northern tropical Atlantic region [*Misra and Zhang*, 2006, Figure 3].

[32] A similar correlation of the Niño3 SST index with the surface (1000 hPa) divergence is shown from the NCEP reanalysis and the CONTROL simulation in Figures 10a and 10b. There is a significant, spatially coherent negative correlation over the northern tropical Atlantic region displayed by both the NCEP reanalysis and the CONTROL simulation. This colocates with the corresponding northern tropical Atlantic SST anomalies in Figures 9a and 9b and with the corresponding precipitation anomalies (not shown). The EXPT clearly differs from the CONTROL in that there is no spatially coherent signal of the surface convergence over the northern tropical Atlantic region (Figure 10c). One of the main reasons for this discrepancy in the EXPT simulation is a result of the erroneous appearance of the tropical Atlantic SST covariability in both hemispheres with the Niño3 SST index (Figure 9c). The apparent organization of the surface convergence anomalies in the northern tropical Atlantic associated with the Niño3 SST index variability in the NCEP reanalysis and the CONTROL simulation stems from a similar correlation found in the downwelling shortwave flux at the surface shown in Figures 11a and 11b, respectively. The NCEP reanalysis and the CONTROL indicate a significant negative correlation over the northern tropical Atlantic region that coincides with similar correlations found with the SST (Figure 9) and

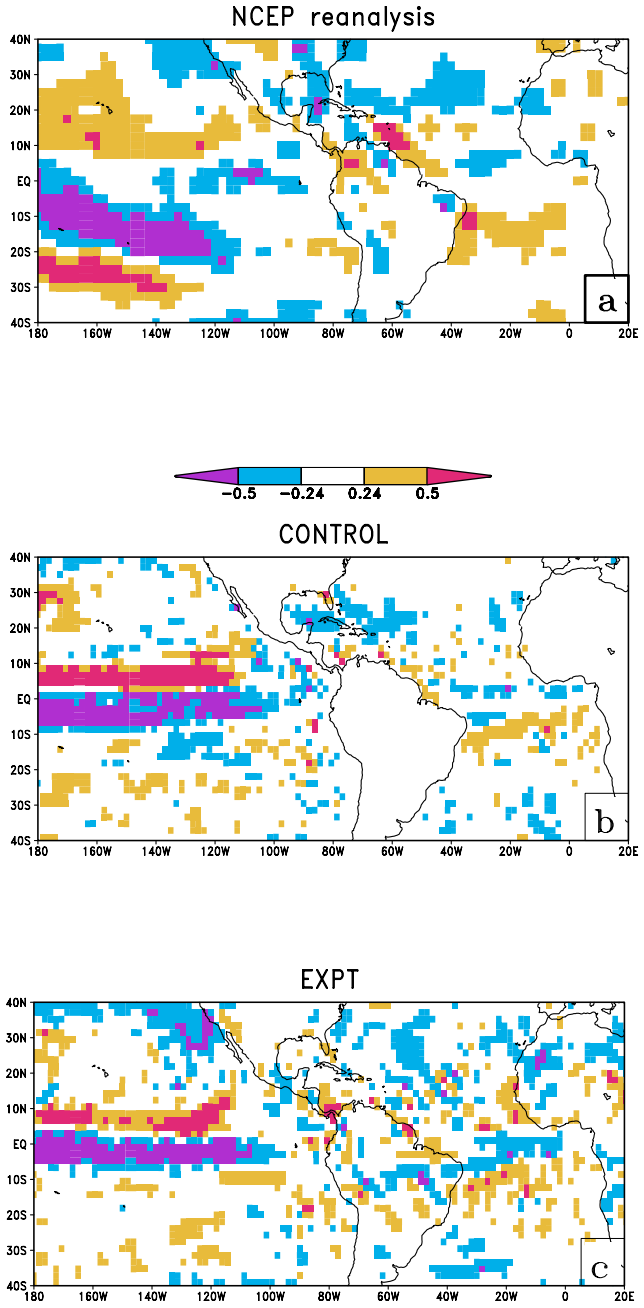

Figure 10. The correlation of the Niño3 SST index averaged over the FMA season with contemporaneous surface (1000 hPa) convergence from (a) NCEP reanalysis, (b) CONTROL, and (c) EXPT. Values that exceed 90% confidence interval according to *t* test are shown.

surface convergence (Figure 10) anomalies associated with the Niño3 SST index variations. The negative correlations over the northern tropical Atlantic region in Figures 11a and 11b would suggest that the warm Niño3 SST anomalies are associated with reduced downwelling shortwave flux at surface. Such a spatially coherent negative correlation over the northern tropical Atlantic region is not observed in the EXPT (Figure 11c). This modulation of the downwelling shortwave flux at surface in the northern tropical Atlantic region in the CONTROL run is largely from the variations of the in situ convective clouds associated with the external forcing of the variability in the eastern equatorial Pacific region. This is illustrated in Figure 12a which shows the correlation of the February–April seasonal mean Niño3 SST index with the corresponding vertically integrated (through the model atmosphere depth) convective cloud fraction from the CONTROL simulation. In Figures 12b and 12c we show similar correlations of the February–April

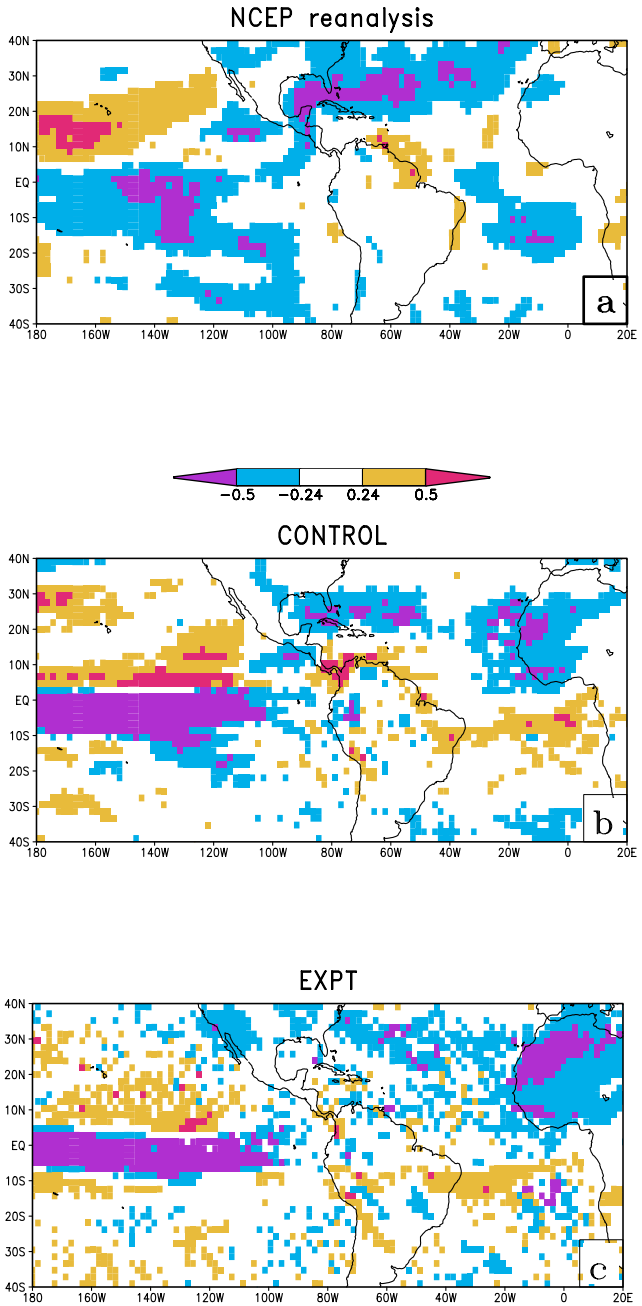

Figure 11. The correlation of the Niño3 SST index averaged over the FMA season with contemporaneous global downwelling shortwave flux from (a) NCEP reanalysis, (b) CONTROL, and (c) EXPT. Values that exceed 90% confidence interval according to *t* test are shown.

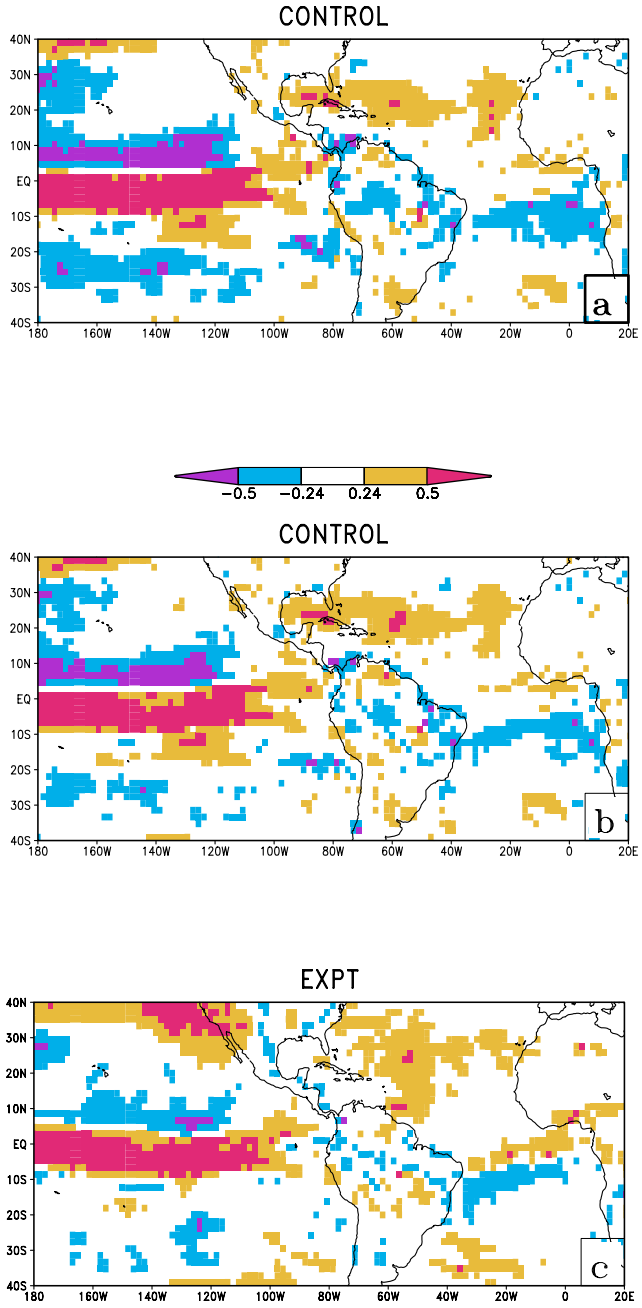

Figure 12. The correlation of the Niño3 SST index averaged o ver the FMA season with contemporaneous (a) vertically integrated (through the depth of the model atmosphere) convective cloud fraction from the CONTROL simulation, (b) convective part of the total precipitation from the CONTROL simulation, and (c) convective part of the total precipitation from the EXPT simulation. Values that exceed 90% confidence interval according to *t* test are shown.

seasonal mean Niño3 SST index with the convective part of the total precipitation from the CONTROL and the EXPT simulations. Since convective cloud fraction was not stored in the EXPT simulation, Figure 12b is shown to prove that convective precipitation is a good proxy to convective cloud fraction in exhibiting its covariability with the Niño3 SST index.

[33] It is clearly suggestive that the difference in the parameterization of the SIC in the EXPT from the CONTROL has resulted in the absence of such correlations of the Niño3 SST index with the downwelling shortwave flux (Figure 11c) and convective cloud precipitation (shown as a proxy to convective cloud fraction in Figure 12c) in the EXPT simulation. In other words, the SIC clouds in the CONTROL simulation regulate a certain organization of the February–April seasonal anomalies of the surface convergence, SST, downwelling shortwave flux at surface and convective clouds over the northern tropical Atlantic region that result in their covariability with the Niño3 SST index variations and a verifiable teleconnection pattern of the February–April seasonal rainfall over the NEB.

4.2.4. The Role of ENSO

[34] *Misra and Marx* [2006] explained the sensitivity of the ENSO simulation to the SIC from the same set of coupled simulations. In that study they showed that in the absence of any smoothing of the SIC (as in EXPT of this paper) the ENSO variability in the tropical Pacific is relatively poor compared to another coupled simulation wherein the SIC is more spatially coherent (as in the CONTROL of this paper). This is best illustrated in Figure 13 which shows the Niño3 SST index spectrum from the observations (ERSST2), CONTROL, and EXPT. The observations show a broad peak in 2.5–7 years range. The CONTROL has a relatively sharp peak centered around 3 years indicating that ENSO is more periodic than what the observations show. The Niño3 SST index spectrum of the EXPT is nearly flat and outside the confidence interval of the observed spectrum. In other words, the ENSO variability in EXPT is relatively very weak.

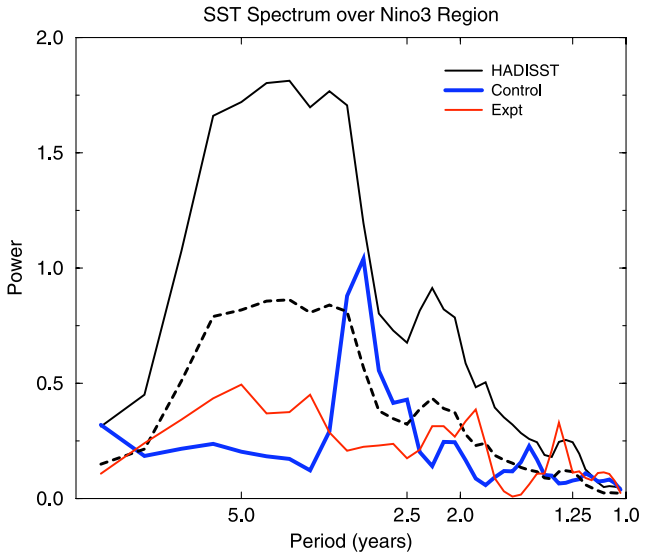

Figure 13. The sample spectrum of monthly mean SST anomalies over the Niño3 region using 45 years of data from observations (ERSST2) and the coupled simulations of the CONTROL and EXPT. The dashed line in the figure shows the lower limit of the 95% confidence interval of the observed sample spectrum for 4 *df* (chosen on the basis of the observed spectrum) according to chi-square test. This gure is borrowed from Misra and Marx (2006).

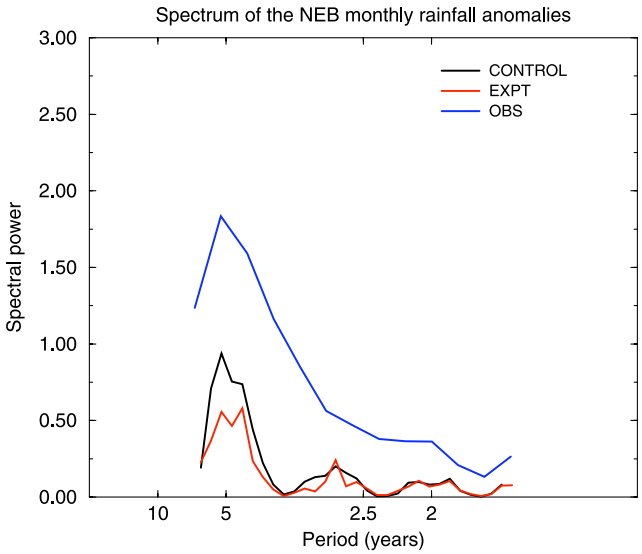

Figure 14. The sample spectrum of the NEB monthly precipitation anomalies from the CONTROL and EXPT model integrations and the OBS(CMAP).

[35] In the EXPT simulation, with ENSO variability being relatively very weak the intrinsic variability of the coupled model (at interannual scales) dominate its influence on the northeast Brazil rainfall variability. This can be justified from the fact that despite any strong SST forcing in the EXPT (Figure 8d), the standard deviation of the interannual monthly mean precipitation anomalies over NEB is comparable in the two coupled simulations (Figures 3b and 3c). Furthermore, the spectrum of the NEB rainfall from the two simulations shown in Figure 14 is nearly the same. This spectrum was calculated by passing the monthly mean precipitation time series through a 3-month running mean filter to make the time series less noisier. The temporal variability is nearly identical in the two model integrations with the spectral power being less than the observations at all temporal scales. The difference in the spectral power at interannual scales (5 years) between the two simulations are not statistically significant.

[36] Therefore this study offers a comparison of two coupled simulations, one with relatively strong and the other relatively weak ENSO like variability in the tropical Pacific. This type of comparison is similar to some of the earlier studies conducted with the uncoupled (to ocean) AGCM integrations [*Misra*, 2005; *Sarvanan and Chang*, 2000; *Giannini et al.*, 2004]. Typically, in these AGCM studies climatological SST was prescribed in one basin (Pacific or the Atlantic) while in the rest of the oceans observed SST was used to understand the sensitivity of the regional SST anomalies. These AGCM studies emphasized the dominating role played by the northern tropical Atlantic SST anomalies while suggesting a subordinate nature of the role played by ENSO in determining the observed teleconnection patterns of the NEB rainfall variability. But as *Misra* [2005] pointed that this conclusion may be unique to uncoupled (to ocean) AGCM experiments that underplay the role of the remote forcing of ENSO variability on northern tropical Atlantic SST anomalies.

[37] This study clearly demonstrates that in the absence of relatively strong ENSO like variability in the coupled model (as in the EXPT), the teleconnections of the NEB rainfall variability with the northern tropical Atlantic SST anomalies are nonexistent. Therefore the well-known predictable teleconnection pattern of the NEB rainfall variability with the eastern equatorial Pacific and the northern tropical Atlantic SST anomalies are closely tied to the ENSO variability.

5. Summary and Conclusions

[38] This study highlights the role of the parameterization of the shallow inversion clouds (SIC) in the context of the annual cycle and the interannual variability of February–March–April (February–April) seasonal rainfall over the northeast Brazil (NEB). This is achieved by analyzing two long-term coupled simulations that differed in the parameterization of the SIC. The difference in the parameterization amounted to the order of smoothing of the SIC, motivated by spurious spectral effects. The change mimics similar effects on SIC that could be achieved from the amount of smoothing of the model orography, or from the choice of the dynamical core (with some schemes being implicitly more diffusive than others), or from the choice of the horizontal and vertical resolution of the AGCM which could either exacerbate or damp the spectral effects by triggering the "on-off" switches in the parameterization scheme.

[39] It is found that the presence of coherent (incoherent) SIC in the CONTROL (EXPT) simulation in the tropical Atlantic decreases (increases) the downwelling shortwave flux, and lowers (raises) the SST. This in turn modulates the surface pressure gradient which produces associated changes to the surface convergence and precipitation over the ITCZ. Most importantly the dominating mechanism of precipitation generation in the tropical Atlantic changes from a thermodynamic (in CONTROL) to dynamic control (in EXPT). In this study it is found that the surface convergence and precipitation over the Atlantic ITCZ is increased in the CONTROL relative to the EXPT. Concomitantly the CONTROL (EXPT) exhibits a wetter (drier) rainy season over the NEB.

[40] In contrast to the larger sensitivity of precipitation over the Atlantic ITCZ to SIC in the August–October season compared to the February–April season, the annual cycle of precipitation over the northeast Brazil (NEB) shows larger differences in the wet season of February–April than in the dry season of August–October. This is simply because in August–October the Atlantic ITCZ is relatively more remote from NEB than in February–April.

[41] The NEB interannual precipitation variability in February–April season has a relatively high predictability owing to its teleconnection with the variability in the neighboring tropical Pacific and Atlantic Oceans. Although many simulation studies of the past that used observed SST to force their AGCM were able to demonstrate this high predictability of seasonal rainfall over the NEB, the coupled models have not shown similar promise.

[42] The CONTROL simulation with more realistic SIC [*Misra and Marx*, 2006] displayed the well-known teleconnection of the February–April seasonal rainfall over the NEB with the contemporaneous SST anomalies in the eastern equatorial Pacific and northern tropical Atlantic

Oceans. The SST anomalies in the northern tropical Atlantic serve a critical role in mediating the SST variability over the eastern equatorial Pacific to the NEB rainfall variations. Other related variables such as the surface convergence, downwelling shortwave flux at surface, convective cloud fraction over the northern tropical Atlantic region show significant correlations with the SST variability over the eastern equatorial Pacific region both in the observations and in the CONTROL simulation. On the other hand, the EXPT simulation that had uncorrected spectral effects in the SIC showed covariability of the NEB rainfall with only the eastern equatorial Pacific SST anomalies. Consequently, the covariability of SST, surface convergence, downwelling shortwave flux at surface over the northern tropical Atlantic region with eastern equatorial Pacific SST anomalies is absent in the EXPT simulation.

[43] The differences in the teleconnection patterns of the NEB rainfall variability between the CONTROL and the EXPT is attributed to the different ENSO characteristics of the two. In the CONTROL the Niño3 SST spectrum has a strong 3-year peak while in the EXPT it is nearly flat and outside the confidence interval of the observed spectrum.

[44] It is to be however noted that the interannual variability over the NEB is not completely dictated by these teleconnection patterns over the tropical Atlantic and Pacific Oceans. A significant variation of the NEB rainfall is also due to the intrinsic modes of the tropical Atlantic Ocean which have not been addressed in this study.

[45] **Acknowledgments.** This study was supported by NSF grant ATM0332910, NASA grant NNG04GG46G, and NOAA grant NA04OAR4310034.

References

Bacmeister, J., et al. (2000) An atlas of seasonal means simulated by the NSIPP-1 atmospheric GCm. 17, NASA Tech Memo 104606, 194 pp., Goddard Space Flight Center, Greenbelt, MD.

Biasutti, M., D. S. Battisti, and E. S. Sarachik (2003), The annual cycle over the tropical Atlantic, South America, and Africa, *J. Clim.*, *16*, 2491–2508.

Biasutti, M., D. S. Battisti, and E. S. Sarachik (2004), Mechanisms controlling the annual cycle of precipitation in the tropical atlantic sector in an atmospheric GCM, *J Clim.*, *17*, 4708–4723.

Biasutti, M., D. S. Battisti, and E. S. Sarachik (2005), Terrestrial influence on the annual cycle of the Atlantic ITCZ in an AGCM coupled to a slab ocean model, *J Clim.*, *18*, 211–228.

Biasutti, M., A. H. Sobel, and Y. Kushnir (2006), AGCM precipitation biases in the tropical Atlantic, *J Clim.*, *19*, 935–958.

Briegleb, B. P. (1992), Delta-Eddington approximation for solar radiation in the NCAR community climate model, *J. Geophys. Res.*, *97*, 7603–7612.

Cazes-Boezio, G., A. W. Robertson, and C. R. Mechoso (2003), SEasonal dependence of ENSO teleconnections over South America and relationships with precipitation in Uruguay, *J. Clim.*, *16*, 1159–1176.

Chang, P., R. Saravanan, and L. Ji (2003), Tropical Atlantic seasonal predictability: the roles of El Niño remote influence and thermodynamic air-sea feedback, *Geophys. Res. Lett.*, *30*(10), 1501, doi:10.1029/2002GL016119.

Collins, W. D., J. K. Hackney, and D. P. Edwards (2002), A new parameterization for infrared emission and absorption by water vapor in the National Center for Atmospheric Research Community Atmosphere Model, *J. Geophys. Res.*, *107*(D22). 4464, doi:10.1029/2001JD001365.

Dirmeyer, P. A., and F. J. Zeng (1999), Precipitation infiltration in the simplified SiB land surface scheme, *J. Meteorol. Soc. Jpn.*, *78*, 291–303.

Enfield, D. B., and D. A. Mayer (1997), Tropical Atlantic sea surface temperature variability and its relation to El Niño Southern Oscillation, *J. Geophys. Res.*, *102*, 929–945.

Fennessy, M. J., et al. (1994), The simulated Indian monsoon: A GCM sensitivity study, *J. Clim.*, *7*, 33–43.

Folland, C. K., A. W. Colman, D. P. Rowell, and M. K. Davey (2001), Predictability of northeast Brazil rainfall and real-time forecast skill, 1987–98, *J. Clim.*, *14*, 1937–1958.

Giannini, A., J. C. H. Chang, M. A. Cane, Y. Kushnir, and R. Seager (2001), The ENSO teleconnection of the tropical Atlantic Ocean: Contributions of the remote and local SST's to rainfall variability in the tropical Americas, *J. Clim.*, *14*, 4530–4544.

Giannini, A., R. Saravanan, and P. Chang (2004), The preconditioning role of tropical Atlantic variability in the development of the ENSO teleconnection: Implications for the prediction of Nordeste rainfall, *Clim. Dyn.*, *22*, 839–855, doi:10.1007/s00382-004-0420-2.

Goddard, L., A. G. Barnston, and S. J. Mason (2003), Evaluation of the IRI's "net assessment" seasonal climate forecasts: 1997–2001, *Bull. Am. Meteorol. Soc.*, *84*, 1761–1781.

Hastenrath, S., and L. Heller (1977), Dynamics of climate hazards in northeast Brazil, *Q. J. R. Meteorol. Soc.*, *103*, 77–92.

Hong, S. Y., and H. L. Pan (1996), Nonlocal boundary layer vertical diffusion in a medium range forecast model, *Mon. Weather Rev.*, *124*, 2322–2339.

Huang, B., P. S. Schopf, and J. Shukla (2005), Intrinsic ocean-atmosphere variability of the tropical Atlantic Ocean, *J. Clim.*, *18*, 1652–1672.

Kalnay, E., et al. (1996), The NCEP/NCAR 40-year reanalysis project, *Bull. Am. Meteorol. Soc.*, *77*, 437–471.

Kayano, M. T., and R. V. Andreoli (2006), Relationships between rainfall anomalies over northeastern Brazil and El Niño–Southern Oscillation, *J. Geophys. Res.*, *111*, D13101, doi:10.1029/2005JD006142.

Kiehl, J. T., J. J. Hack, G. Bonan, B. A. Boville, D. L. Williamson, and P. J. Rasch (1998), The National Center for Atmospheric Research Community Climate Model: CCM3, *J. Clim.*, *11*, 1131–1149.

Levitus, S. (1982), Climatological World Atlas of the Ocean, U. S. Govt. Printing Office, 173 p.

Li, T., and S. G. H. Philander (1997), On the seasonal cycle of the equatorial Atlantic Ocean, *J Clim.*, *10*, 813–817.

Lindzen, R. S., and S. Nigam (1987), On the role of the sea surface temperature gradients in forcing low-level winds and convergence in the tropics, *J. Atmos. Sci.*, *44*, 2418–2436.

Misra, V. (2004), An evaluation of the predictability of austral summer season precipitation over South America, *J. Clim.*, *17*, 1161–1175.

Misra, V. (2005), Understanding the predictability of seasonal precipitation over northeast Brazil, *Tellus*, *58A*, 307–319.

Misra, V. (2006), Understanding the predictability of seasonal precipitation over northeast Brazil, *Tellus*, *58A*, 307–319.

Misra, V., and L. Marx (2006), Role of the Inversion Clouds in a Coupled Model Simulation over the Equatorial Pacific Ocean. Part II: Sensitivity of ENSO Variability, COLA Technical report #219. Available from ftp://grads.iges.org/pub/ctr/ctr_219.pdf, 30 p.

Misra, V., and Y. Zhang (2006), The fidelity of NCEP-CFS seasonal hindcasts over Nordeste, *Mon. Weather Rev.*, in press.

Misra, V., et al. (2006), Validating ENSO simulation in coupled climate models. COLA technical report #210, Available from ftp://grads.iges.org/pub/ctr/ctr_210.pdf.

Mo, K. C., and R. W. Higgins (1998), The Pacific-South American modes and tropical convection during the Southern Hemisphere winter, *Mon. Weather Rev.*, *126*, 1581–1596.

Moura, A. D., and J. Shukla (1981), On the dynamics of droughts in northeast Brazil: Observations, theory and numerical experiments with a general circulation model, *J. Atmos. Sci.*, *38*, 2653–2675.

Neelin, J. D., and H. Su (2005), Moist teleconnection mechanisms for the tropical South American and Atlantic Sector, *J. Clim.*, *18*, 3928–3950.

Nobre, C., and J. Shukla (1996), Variations of sea surface temperature, wind stress, and rainfall over the tropical Atlantic and South America, *J. Clim.*, *9*, 2464–2479.

Pacanowski, R. C., and S. M. Griffies (1998), MOM3.0 manual, NOAA/Geophysical Fluid Dynamics Laboratory, Princeton, New Jersey, USA 08542.

Philander, S. G. H., D. Gu, G. Lambert, T. Li, D. Halpern, N.-C. Lau, and R. C. Pacanowski (1996), Why the ITCZ is mostly north of the equator, *J. Clim.*, *9*, 2958–2972.

Raymond, D., G. Raga, C. Bretherton, J. Molinari, C. Lopez-Carrillo, and Z. Fuchs (2003), Convective forcing in the intertropical convergence zone of the eastern Pacific, *J. Atmos. Sci.*, *60*, 2064–2082.

Saha, S., et al. (2006), The NCEP climate forecast system, *J. Clim.*, In press.

Sarvanan, R., and P. Chang (2000), Interaction between tropical Atlantic variability and El Niño–Southern Oscillation, *J. Clim.*, *13*, 2177–2194.

Schneider, E. K. (2002), Understanding differences between the equatorial Pacific as simulated by two coupled GCMs, *J. Clim.*, *15*, 449–469.

Smith, T. M., and R. W. Reynolds (2003), Extended reconstruction of global sea surface temperatures based on COADS data (1854–1997), *J. Clim.*, *16*, 1495–1510.

Sun, L., D. F. Moncunill, H. Li, A. D. Moura, and F. D. A. D. S. Filho (2005), Climate downscaling over Nordeste, Brazil, using the NCEP RSM97, *J. Clim.*, *18*, 551–567.

Sun, L., D. F. Moncunill, H. Li, A. D. Moura, F. D. A. D. S. Filho, and S. E. Zebiak (2006), An operational dynamical downscaling prediction system for Nordeste Brazil and the 200204 real-time forecast evaluation, *J. Clim.*, *19*, 1990–2007.

Tiedtke, M. (1984), The effect of penetrative cumulus convection on the large-scale flow in a general circulation model, *Beitr. Phys. Atmos.*, *57*, 216–239.

Tomas, R., J. Holton, and P. Webster (1999), The influence of cross-equatorial pressure gradients on the location of near equatorial convection, *Q. J. R. Meteorol. Soc.*, *125*, 1107–1127.

Xie, P., and P. Arkin (1996), Analysis of global monthly precipitation using guage observations, satellite estimates and numerical model predictions, *J. Clim.*, *9*, 840–858.

Xue, Y.-K., P. J. Sellers, J. L. Kinter III, and J. Shukla (1991), A simplified Biosphere Model for global climate studies, *J. Clim.*, *4*, 345–364.

Xue, Y.-K., F. J. Zeng, and C. A. Schlosser (1996), SSiB and its sensitivity to soil properties, A case study using HAPEX-Mobilhy data, *Global Planet. Change*, *13*, 183–194.

V. Misra, Center for Ocean-Land-Atmosphere Studies Institute of Global Environment and Society, Inc., 4041 Powder Mill Road, Suite 302, Calverton, MD 20705, USA. (misra@cola.iges.org)